The American Journal of Pathology, Vol. 193, No. 10, October 2023

ELSEVIER

The American Journal of
PATHOLOGY
ajp.amjpathol.org

CARDIOVASCULAR, PULMONARY, AND RENAL PATHOLOGY

Tryptophan Metabolites Target Transmembrane and Immunoglobulin Domain-Containing 1 Signaling to Augment Renal Tubular Injury

Mostafa Belghasem,* Wenqing Yin,† Saran Lotfollahzadeh,† Xiaosheng Yang,† Rosana D. Meyer,* Marc A. Napoleon,† Isaac E. Sellinger,† Aniket Vazirani,†‡ Elena Metrikova,* Asha Jose,† Anna Zhebrun,† Stephen A. Whelan,‡§ Norman Lee,‡§ Nader Rahimi,* and Vipul C. Chitalia†¶‖**

From the Departments of Pathology and Laboratory Medicine and Surgery,‡ and the Renal Section† and the Center of Cross-Organ Vascular Pathology,** Department of Medicine, Boston Medical Center, Boston University School of Medicine, Boston; the Chemistry Instrumentation Core,§ School of Chemistry, Boston University, Boston; the Veterans Affairs Boston Healthcare System,¶ Boston; and the Institute of Medical Engineering and Science,‖ Massachusetts Institute of Technology, Cambridge, Massachusetts*

Accepted for publication June 29, 2023.

Address correspondence to Vipul C. Chitalia, M.D., Ph.D., Center of Cross-Organ Vascular Pathology, Renal Section, Department of Medicine, Boston University Medical Center, 650 Albany St., EBRC X545, Boston, MA 02118.
E-mail: vichital@bu.edu.

Chronic kidney disease (CKD) is characterized by the accumulation of uremic toxins and renal tubular damage. Tryptophan-derived uremic toxins [indoxyl sulfate (IS) and kynurenine (Kyn)] are well-characterized tubulotoxins. Emerging evidence suggests that transmembrane and immunoglobulin domain-containing 1 (*TMIGD1*) protects tubular cells and promotes survival. However, the direct molecular mechanism(s) underlying how these two opposing pathways crosstalk remains unknown. We posited that IS and Kyn mediate tubular toxicity through TMIGD1 and the loss of TMIGD1 augments tubular injury. Results from the current study showed that IS and Kyn suppressed TMIGD1 transcription in tubular cells in a dose-dependent manner. The wild-type CCAAT enhancer-binding protein β (C/EBPβ) enhanced, whereas a dominant-negative C/EBPβ suppressed, *TMIGD1* promoter activity. IS down-regulated C/EBPβ in primary human renal tubular cells. The adenine-induced CKD, unilateral ureteric obstruction, and deoxycorticosterone acetate salt unilateral nephrectomy models showed reduced TMIGD1 expression in the renal tubules, which correlated with C/EBPβ expression. C/EBPβ levels negatively correlated with the IS and Kyn levels. Inactivation of TMIGD1 in mice significantly lowered acetylated tubulin, decreased tubular cell proliferation, caused severe tubular damage, and worsened renal function. Thus, the current results demonstrate that TMIGD1 protects renal tubular cells from renal injury in different models of CKD and uncovers a novel mechanism of tubulotoxicity of tryptophan-based uremic toxins. *(Am J Pathol 2023, 193: 1501–1516; https://doi.org/10.1016/j.ajpath.2023.06.018)*

Chronic kidney disease (CKD) affects nearly 10% to 15% of the world's population and 40 million adult Americans. It possesses an astronomical health care and economic burden.[1,2] Patients with CKD experience a relentless deterioration of renal function, culminating in end-stage kidney disease in a process mainly driven by the loss of functional renal tubular mass. Despite the importance of tubular cell protection, the current management of patients with CKD has few agents that directly protect renal tubular epithelial cells (RTECs).

Supported in part by the American Heart Association (AHA) Career Development Award number 850917 (W.Y.); NIH grants R01HL132325, R21DK119740, R01HL166608-01A1, and R21DK132784 (V.C.C.) and R21CA191970 and R21CA193958 (N.R.); AHA Cardio-Oncology Strategically Focused Research Networks Cancer-Associated Thromboembolism as Affected by Health Disparities (CAT-HD) Center grant 857078 (A.J., V.C.C., X.Y., and S.L.); and the Center of Cross-Organ Vascular Pathology at Boston University Department of Medicine (V.C.C.).

M.B. and W.Y. are joint first authors.

Disclosures: None declared.

A portion of this work was presented at the 2018 annual meeting of the American Society of Nephrology, San Diego, CA, October 23–28, 2018.

https://doi.org/10.1016/j.ajpath.2023.06.018

CKD is uniquely characterized by the retention of uremic solutes,[3] which are retained from the early stages of CKD,[4–6] and their levels substantially increase with the progression of CKD. The protein-bound nature of some uremic toxins precludes clearance by hemodialysis. A wealth of epidemiologic studies have demonstrated the association of protein-bound uremic toxins with systemic complications of patients with CKD. These studies are supported by work in preclinical models, demonstrating their causal association with cardiovascular diseases; and as a result, protein-bound uremic toxins are now considered emerging therapeutic targets.[7] Epidemiologic studies have shown a correlation between the levels of uremic toxins, especially indolic solutes [indoxyl sulfate (IS) and indoxyl acetate (IA)], and the progression of CKD, suggesting their possible tubulotoxic effects.[4–6] However, little is known about the tubulotoxicity of tryptophan metabolites.

We have previously identified transmembrane and immunoglobulin domain containing 1 (TMIGD1).[8,9] TMIGD1 is predominantly expressed in the cytosol and membrane of RTECs[9] and also detected in the mitochondria.[10] TMIGD1 protects RTECs from cell injury in response to oxidative stress and nutritional deprivation.[9] Further probing of a rodent CKD model showed downregulation of TMIGD1 mRNA in kidneys,[8] suggesting a renoprotective function for TMIGD1.[9,10] We therefore investigated a possible crosstalk between the uremic tubulotoxin solutes and the renoprotective function of TMIGD1 pathway in CKD.

Materials and Methods

TMIGD1 Heterozygous and Homozygous Knockout Models

Development and characterization of whole body homozygous TMIGD1 KO mice were previously described.[9] TMIGD1 heterozygous mice were generated at the Nanjing BioMedical Research Institute of Nanjing University (Nanjing, China) on a C57BL/6J background. Mice used in this study were bred and maintained at Boston University Medical Center (Boston, MA) after approval from the Institutional Animal Care and Use Committee. The following primers were used for genotyping of TMIGD1 mice: forward primer, 5′-CCCTATATCCTCAGGCTCTG-3′; and reverse primer, 5′-CGTTCAGCACTACTG-TAACGGAC-3′.[9]

Adenine-Induced CKD Model

To evaluate the expression of TMIGD1 in an adenine-induced model of chronic kidney disease, a group of 12-week−old male and female C57BL/6J mice ($n = 4$) was fed a normal diet (Teklad Global 18% Protein Rodent Diet; Envigo, Indianapolis, IN) supplemented with 0.2% adenine (Research Diets, New Brunswick, NJ) for 14 days.

Unilateral Ureteric Obstruction Model

A group of 12-week−old C57BL/6 and TMIGD1 KO mice underwent laparotomy and left ureter ligation proximal to the urinary bladder. A group of mice was harvested at 1, 2, and 3 weeks after the procedure, and both obstructed (ligated) and unobstructed kidneys were isolated. The kidneys were sectioned through the hilum along the vertical axis. Sections were then processed, paraffin embedded, and sectioned for staining.

DOCA-Salt and Unilateral Nephrectomy Model

A group of 12-week−old C57BL/6 and TMIGD1 KO mice underwent laparotomy and left kidney resection, followed by deoxycorticosterone acetate (DOCA) salt pellet implantation. Animals were harvested 6 weeks after the procedure, and the remaining kidney was sectioned through the hilum along the vertical axis. Sections were then processed, paraffin embedded, and sectioned for staining.

TMIGD1 Promoter-Reporter Assay

HEK293T cells were transfected with TMIGD1-luciferase reporter construct, as described previously.[10] Cells were treated with different compounds after 24 hours of transfection. Luciferase assays were performed after 24 hours of treatment using the Dual-Luciferase kit (Promega, Madison, WI), and luciferase values were normalized to protein content, determined by the Bradford assay (Bio-Rad, Hercules, CA). A detailed method is described elsewhere.[7]

Cell Culture, Reagents, and Immunoblotting

The primary RTECs (Lonza, Lexington, MA; number CC-2556) were cultured in REGM Renal Epithelial Cell Growth Medium (Lonza), along with the growth BulletKit (Lonza), 10% fetal bovine serum, and 10% streptomycin, and incubated in a humidified atmosphere of 5% CO_2 at 37°C. BUMPT and HEK293T cells were grown in Dulbecco's modified Eagle's medium + 10% fetal bovine serum and 1% penicillin and streptomycin. Cells were incubated with IS (Sigma-Aldrich, St. Louis, MO; I3875) or IA (Sigma-Aldrich; I3500) and dimethyl sulfoxide (Sigma, St. Louis, MO) as control. Immunoblots were performed as described previously.[11]

IF, Antibodies, and Image Quantification

For immunofluorescence (IF) staining, tissue was harvested, sectioned (5 μm thick), and fixed in formaldehyde or paraformaldehyde, using conventional procedures. Rabbit polyclonal anti-TMIGD1 antibody was used at 1:100 dilution and incubated overnight at 4°C, which was made against a peptide that corresponded to 20 amino acids in the extracellular domain of TMIGD1, as described.[8] The

authors used rabbit anti−CCAAT enhancer-binding protein β (C/EBPβ) antibody from Cell Signaling (Danvers, MA; catalog number 3087) at 1:1000 dilution (for immunoblotting) and 1:50 dilution (for IF), incubated overnight at 4°C. Acetyl-α-tubulin (Lys40; Cell Signaling; 5335) at 1:100 dilution, proliferating cell nuclear antigen (PCNA; Cell Signaling; 13110) at 1:200 dilution, and Ki-67 (Cell Signaling; 9449) at 1:100 dilution were used for IF. The secondary antibodies consisted of Alex Fluor 488, 594, and 647 (Molecular Probes, Eugene, OR) at 1:250 dilution for 45 minutes at room temperature. For Western blot analyses, the authors used the following antibodies: TMIGD1 (1:1000), glyceraldehyde-3-phosphate dehydrogenase (Cell Signaling; 2118S; 1:5000), kidney-specific (Ksp) cadherin (Novus Biologicals, Centennial, CO; NBP2-45157): 1:1000, N-cadherin (Novus Biologicals; NBP1-48309; 1:1000), and C/EBPβ (Cell Signaling; 3082S).

For image quantification on IF, the entire slide was scanned by a motorized stage system using the Nikon (Melville, NY) NIS Elements software version 5.30.05 at the Boston University School of Medicine Imaging core. The images were processed in ImageJ software version 1.53 (NIH, Bethesda, MD; *https://imagej.nih.gov/nih-image*, last accessed June 13, 2023), where the signal was converted to grayscale, the number and intensity of pixels were analyzed as integrated density using the plugin Fiji, and the region of interest was defined. The integrated density of all the images was normalized to their area. Image quantification was quantitated using ImageJ software.

Renal Function Evaluation

Renal function was assessed on terminal plasma from all mice by measuring blood urea nitrogen (BUN). BUN was determined by following manufacturer's protocol using a Quantichrom Urea Assay Kit (DIUR-100) from Bioassay Systems (Hayward, CA). Absorbance was measured using a Quant 96-well plate reader (Bio-Tek Instruments, Inc, Winooski, VT). Samples were analyzed in duplicate, with the average BUN determined.

Chemical reagents are included in Supplemental Table S1.

All these compounds were dissolved in dimethyl sulfoxide.

Nuclear Subcellular Fractionation

Cells were dounce (Kontes, Vineland, NJ) homogenized in cytosol lysis buffer (250 mmol/L sucrose, 10 mmol/L HEPES, pH 7.4, 2.5 mmol/L $MgCl_2$, 0.5 mmol/L EDTA, 100 μmol/L Na_3VO_4, 100 μmol/L phenylmethylsulfonyl fluoride, and complete protease inhibitor; Roche, Marlborough, MA). After two centrifugations at 1000 × *g* for 10 minutes at 4°C, the anucleated supernatant was centrifuged at 100,000 × *g* at 4°C for 30 minutes. The supernatant was removed. The nuclear pellet from the first spin was resuspended in nuclear lysis buffer (50 mmol/L HEPES, pH 7.4, 50 mmol/L KCl, 300 mmol/L NaCl, 0.1 mmol/L EDTA, 100 μmol/L Na_3VO_4, 100 μmol/L phenylmethylsulfonyl fluoride, and complete protease inhibitor; Roche) and followed by three cycles of freeze and thaw. The nuclear fraction was cleared by centrifugation.

Histologic Analysis and Quantification of Renal Tubular Damage

Hematoxylin and eosin and Masson trichrome stains were performed on the slide in the Histopathology Core at Boston University Medical Center. The slides were evaluated by a pathologist (M.B.) blinded to the sample identity. By using a semiquantitative interstitial fibrosis and tubular atrophy (IFTA) scoring method on periodic acid−Schiff−stained sections, tubular atrophy, dilatation, casts, interstitial inflammation, and fibrosis were used as parameters of interstitial damage. IFTA grade 0 indicates no changes; grade 1, lesions involving <25% of the field; grade 2, lesions affecting 25% to 50% of the field; grade 3, lesions affecting 50% to 75% of the field; and grade 4, lesions involving >75% of the field.

Statistical Analysis

Statistical analysis was performed using GraphPad Prism 8 (GraphPad Software, San Diego, CA) or SAS version 9.3 (SAS Institute, Cary, NC). A two-tailed *t*-test was performed for group comparisons. For multiple groups, overall group comparison was first examined using analysis of variance. With the rejection of the null hypothesis, *post hoc* analysis using Bonferroni correction or pairwise comparisons with Tukey multiple-comparison procedure were performed for *in vitro* and *in vivo* studies. Linear regression was performed to correlate two parameters. $P < 0.05$ was considered statistically significant.

Results

The authors first examined whether IS regulates TMIGD1 transcription in renal tubular cells. To this effect, primary human proximal tubular epithelial cells were treated with different concentrations of IS, corresponding to levels seen in patients at different stages of CKD. The *TMIGD1* mRNA was reduced in a dose-dependent manner by IS (Figure 1A). In the same cell lysates, the IS-treated cells showed approximately 50% suppression of TMIGD1 protein (Figure 1, B and C). Other cell membrane proteins (N-cadherin and Ksp-cadherin) were examined in response to IS treatment (Supplemental Figure S1). Prevalidated Boston University mouse proximal tubular epithelial cells (BUMPT)[12–14] were treated with the indicated concentrations of IS, and lysates were probed for Ksp-cadherin, N-cadherin, and TMIGD1. Glyceraldehyde-3-phosphate dehydrogenase (GAPDH) served as a loading control. Ksp-cadherin expression was up-regulated by 50% to 80%

in cells treated with 10 to 50 μmol/L IS, and the levels reduced by 60% with 100 μmol/L IS. No changes in N-cadherin were noticed with IS. TMIGD1 expression was down-regulated with increasing concentration of IS in BUMPT cells. These data suggest that Ksp-cadherin follows a bimodal pattern of alteration in response to IS, which is different from that of TMIGD1. However, at higher levels of IS, both Ksp-cadherin and TMIGD1 underwent similar changes, whereas N-cadherin remained unaltered with IS.

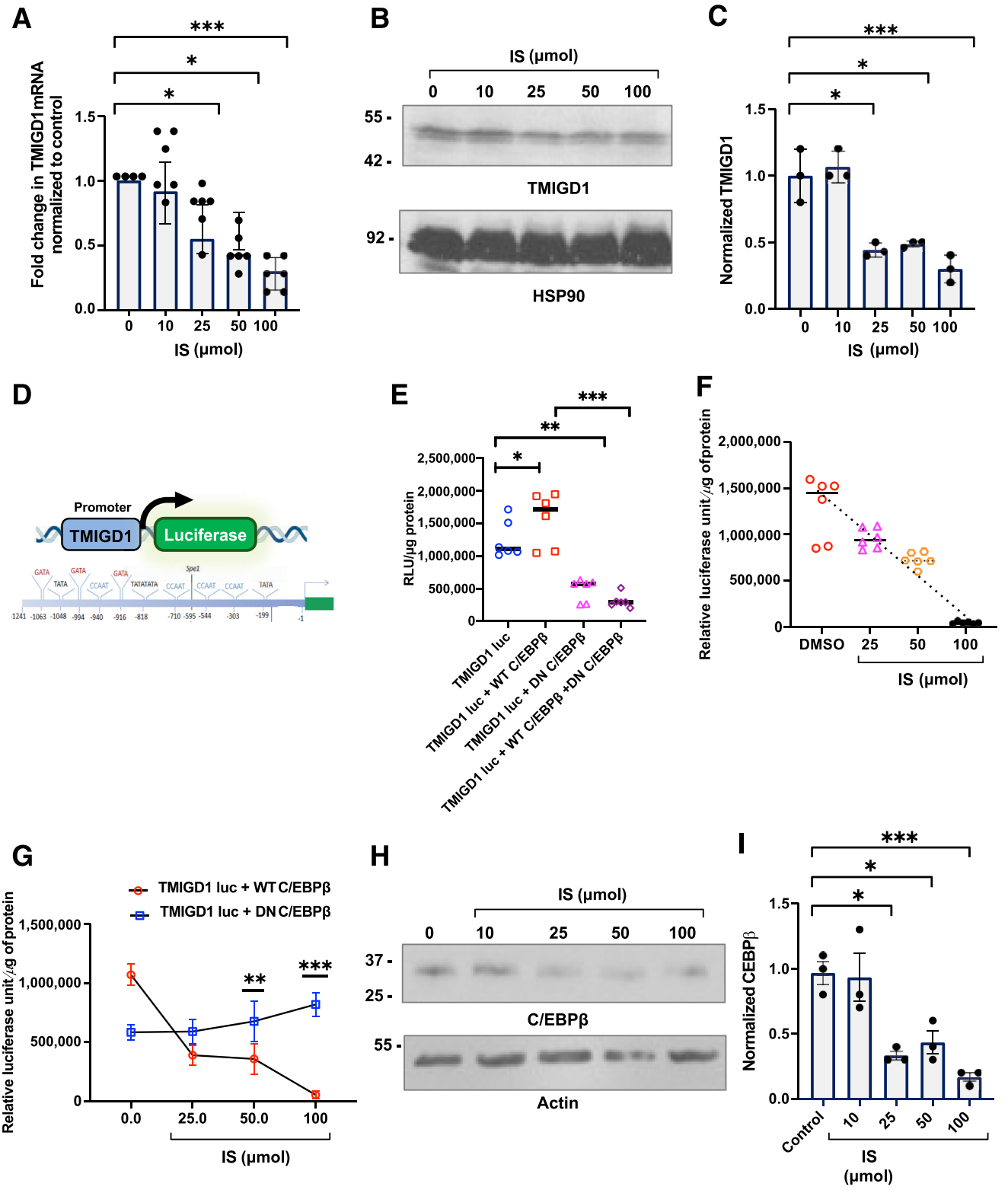

The transcriptional regulation of TMIGD1 by IS was assessed next. The TMIGD1 promoter contains four CCAAT boxes,[9] which are known to bind to CCAAT/enhancer binding family of transcriptional factors [C/EPB; alias liver-enriched transcriptional activator protein (LAP)] (Figure 1D). C/EPB family has 11 transcription factor members, of which C/EPBβ is expressed in kidneys.[15] The authors posited that C/EPBβ regulates the TMIGD1 transcription in RTECs. A promoter-reporter construct of TMIGD1 was generated for this purpose (Figure 1D). This construct contained a 5′-flanking noncoding region of 1241 bp upstream of the transcription start site in the human *TMIGD1* gene with four CCAAT boxes and was tethered to luciferase reporter (Figure 1D). To examine the effect of C/EPBβ, wild-type C/EPBβ and a dominant-negative C/EPBβ (without the transcription of the DNA-binding domain) were co-expressed in HEK293T cells. TMIGD1 transcription was up-regulated by wild-type C/EPBβ and down-regulated by dominant-negative CEPBβ (Figure 1E). Additionally, co-expression of dominant-negative C/EPBβ along with wild-type C/EPBβ significantly reduced the TMIGD1 transcription. These data suggest that C/EPBβ regulates TMIGD1 transcription.

Whether IS regulated TMIGD1 transcription through C/EPBβ was examined next. First, HEK293T cells expressing TMIGD1-luciferase reporter construct were exposed to a titrated concentration of IS (Figure 1F). IS suppressed TMIGD1 transcription in a dose-dependent manner. Second, the TMIGD1-luciferase reporter construct with wild-type and dominant-negative C/EPBβ were co-expressed, and the cells were exposed to IS. TMIGD1 transcription was down-regulated in the presence of wild-type C/EPBβ, which was abrogated in the presence of dominant-negative C/EPBβ (Figure 1G and Supplemental Figure S2). These results suggest that IS regulates TMIGD1 transcription through C/EPBβ.

Because IS suppresses TMIGD1 transcription and C/EPBβ mediates this effect, the authors hypothesized that IS down-regulates the expression of C/EPBβ. Primary human proximal RTECs were treated with increasing concentrations of IS and probed for C/EPBβ. IS down-regulated C/EPBβ levels in a dose-dependent manner (Figure 1H). The densitometry analysis revealed nearly a 50% reduction in C/EPBβ expression when cells were exposed to IS concentrations of >25 μmol/L (Figure 1I) compared with dimethyl sulfoxide−treated cells. Collectively, the data described suggest that IS suppresses TMIGD1 transcription by down-regulating C/EPBβ expression in RTECs.

IS is a metabolite of the amino acid tryptophan. Tryptophan follows two distinct pathways of degradation.[16] A vast proportion of tryptophan is absorbed in the liver and is converted to kynurenine (Kyn). Kyn is further modified to kynurenic acid, quinolinic acid, xanthurenic acid, and anthranilic acid. A small proportion of dietary tryptophan is degraded by the gut microbiome to form indole. On absorption in the portal circulation, indole undergoes further transformation into IS and IA.

Figure 1 Indoxyl sulfate (IS) regulates TMIGD1 transcription through CCAAT enhancer-binding protein β (C/EBPβ) and down-regulates C/EBPβ protein levels. **A:** Early-passage primary human renal cortical epithelial cells were treated for 24 hours with an increasing concentration of IS. Cells treated with dimethyl sulfoxide (DMSO) served as control. Real-time PCR measured the fold of TMIGD1 expression and normalized it with controls. The *t*-test was applied to compare different groups. *P* values are given for DMSO-treated cells (IS, 0.0 μmol/L) compared with IS, 25, 50, and 100 μmol/L. **B:** Early-passage primary human renal cortical epithelial cells were treated for 24 hours with a titrated concentration of IS. The cell lysis was probed for TMIGD1. Heat shock protein 90 (HSP90) served as the marker for the loading control. Cells treated with DMSO served as control. Representative images from three independent experiments are shown. **C:** Densitometry analysis of TMIGD1 normalized to HSP90 levels from three independent experiments was performed, and the average of three experiments is shown. Analysis of variance (ANOVA) with Welch correction was used to compare all four groups, which showed $P = 0.001$. The *t*-test was applied to compare different groups. *P* values are given for DMSO-treated cells (IS, 0.0 μmol/L) compared with IS, 25, 50, and 100 μmol/L. **D:** A schematic of TMIGD1 promoter-luciferase construct. A truncated TMIGD1 promoter with Spe1 restriction site (−1241 to −595 bp) upstream of the *TMIGD1* start site (**black angled arrow**) was cloned upstream of an internal ribosomal entry site and tethered to a luciferase reporter system. **E:** HEK293T cells expressing TMIGD1 promoter-luciferase reporter (TMIGD1 luc) were transiently transfected with Flag-tagged wild-type (WT) C/EBPβ or hemagglutinin (HA)-tagged dominant-negative (DN) C/EBPβ plasmids. The cells were harvested, and lysates were subjected to Promega dual-luciferase assay and normalized to protein content [relative luciferase unit (RLU)]. A scatterplot of two independent experiments done in triplicate is shown. The **line** within each group corresponds to the median value. ANOVA with Welch correction was used to compare all four groups, which showed $P < 0.001$. Groups were further compared using *t*-test, and *post hoc* Bonferroni correction was made for multiple comparisons. *P* values are given for TMIGD1 luc compared with WT C/EBPβ and DN C/EBPβ. *P* value is also given for WT C/EBPβ alone compared with WT C/EBPβ + DN C/EBPβ. Expression of WT and DN C/EBPβ are shown in Supplemental Figure S2. **F:** HEK293T cells expressing TMIGD1 luc were treated with a titrated concentration of IS, and luciferase assay was performed as above. A scatterplot of two independent experiments performed in triplicates is shown. The **line** within each group corresponds to the median value. ANOVA with Welch correction was used to compare all four groups, which showed $P < 0.001$. Groups were further compared using *t*-test. Compared with the control vector, TMIGD1 luc (treated with DMSO) showed a significant increase in the luciferase activity ($P < 0.001$). Groups were further compared using *t*-test, and *post hoc* Bonferroni correction was made for multiple comparisons. Compared with DMSO, IS, 25 μmol/L ($P < 0.05$), and IS, 50 and 100 μmol/L ($P < 0.001$). A linear regression analysis showed $R^2 = 0.71$ and $P < 0.001$. **G:** HEK293T cells co-expressing TMIGD1 luc with WT C/EBPβ or DN C/EBPβ were treated with increasing concentration of IS or DMSO (labeled as IS, 0.0 μmol/L) and the luciferase activity was performed. Averages of six replicates are shown. Compared with WT C/EBPβ treated with DMSO (IS, 0.0 μmol/L), all the concentrations of IS suppressed TMIGD1 luciferase activity. Compared with WT C/EBPβ with no IS, DN C/EBPβ suppressed TMIGD1 luc activity ($P < 0.01$). *P* values are given for DN C/EBPβ compared with cells expressing WT C/EBPβ and treated with IS, 50 and 100 μmol/L. **H:** Early-passage primary human renal cortical epithelial cells were treated with increasing concentrations of IS and lysed. Actin served as a loading control. Cells treated with DMSO served as control. Representative images from three independent experiments are shown. **I:** Densitometry analysis of C/EBPβ normalized to actin levels from three independent experiments was performed, and the average of the three experiments are shown. ANOVA with Welch correction was used to compare all four groups, which showed $P < 0.01$. The *t*-test was applied to compare different groups. *P* values are given for DMSO-treated cells (IS, 0.0 μmol/L) compared with IS, 25, 50, and 100 μmol/L. Error bars indicate SEM (**A**, **C**, **G**, and **I**). $^*P < 0.05$, $^{**}P < 0.01$, and $^{***}P < 0.001$.

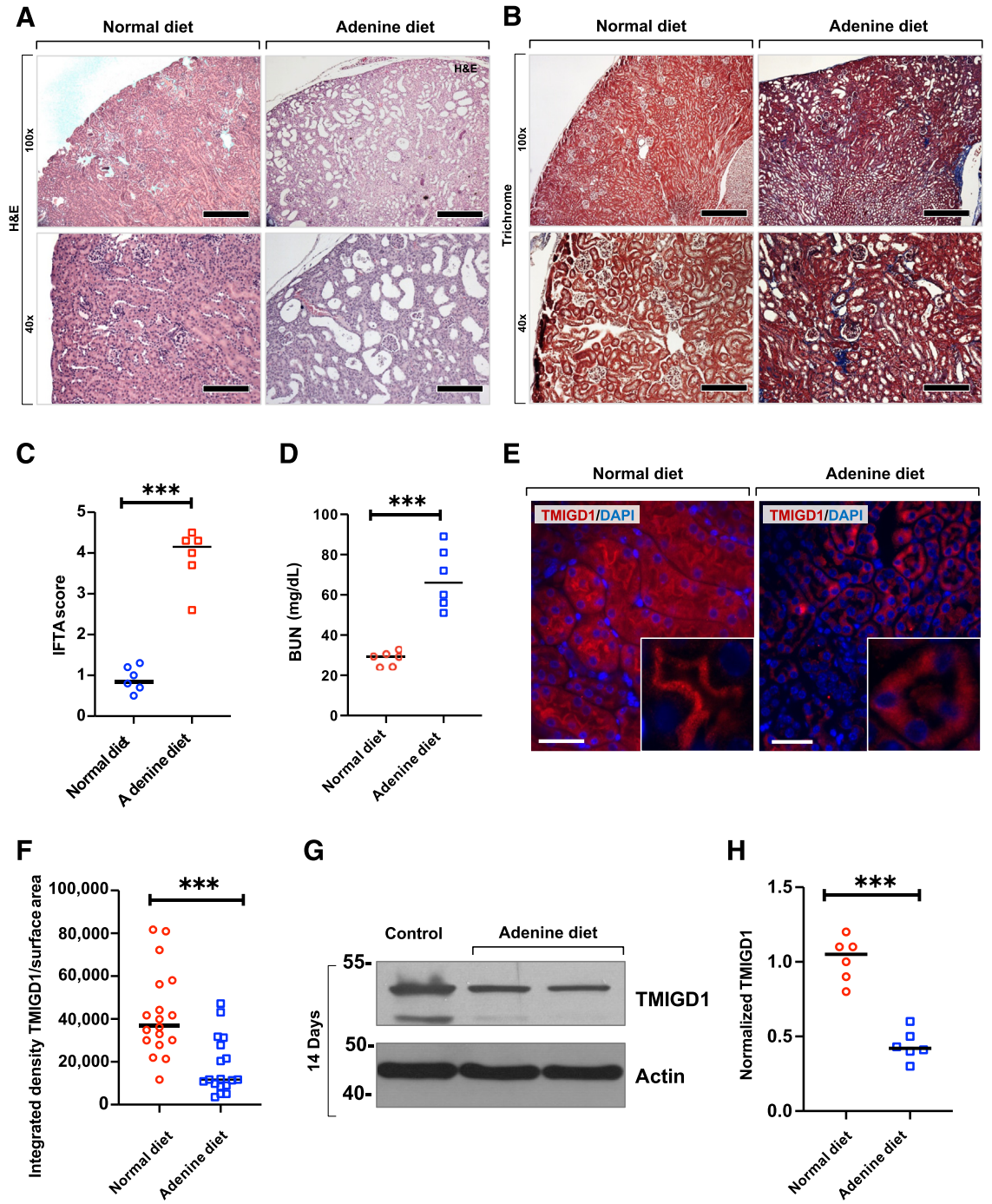

Figure 2 TMIGD1 expression is down-regulated in mice with adenine-induced chronic kidney disease. **A:** A group of male and female C57BL/6 mice was exposed to a 0.2% adenine diet for 4 weeks. The group on a normal diet served as controls. Paraffin-embedded kidney sections were stained with hematoxylin and eosin (H&E), and images are shown at indicated magnification. Representative images from one mouse per group are shown. **B:** Paraffin-embedded kidney sections were stained with modified Masson trichrome stain, and images are shown at indicated magnification. Representative images from one mouse per group are shown. **C:** Interstitial fibrosis and tubular atrophy (IFTA) scores were determined for each mouse (average of two kidneys/mouse) in a manner blinded to the group. The *t*-test was performed. **D:** Blood urea nitrogen (BUN) levels in mice at the end of the experiment are shown. The **line** corresponds to the median. Groups were compared using the *t*-test. **E:** Kidneys harvested from the above mice were stained with TMIGD1 antibody followed by Alexa Fluor secondary antibody. DAPI stained nuclei. Representative images of kidneys from six mice are shown. **Insets:** The apical expression of TMIGD1 from renal tubular cells. **F:** TMIGD1 expression was quantified using integrated density with ImageJ software version 1.53t, and the expression was measured in each tubule, demarcated as a region of interest and normalized to the surface area of a tubule. Three randomly selected images per mouse were analyzed. The **line** corresponds to the median value in each group. The groups were compared using *t*-test. **G:** The kidney lysates of mice harvested at the end of experiments were probed for TMIGD1, and actin served as a loading control. A representative image from the TMIGD1 band from an individual mouse from each group is shown. **H:** Densitometry analysis of the TMIGD1 band normalized to actin was performed for each mouse. The **line** represents the median. The groups were compared using *t*-test. $N = 6$ (**A**, **C**, and **F**, mice on adenine diet and normal diet). $^{***}P < 0.001$. Scale bars: 50 μm (**A** and **B**, **top panels**); 10 μm (**A** and **B**, **bottom panels**); 100 μm (**E**). Original magnifications: ×100 (**A** and **B**, **top panels**); ×40 (**A** and **B**, **bottom panels**); ×200 (**E**).

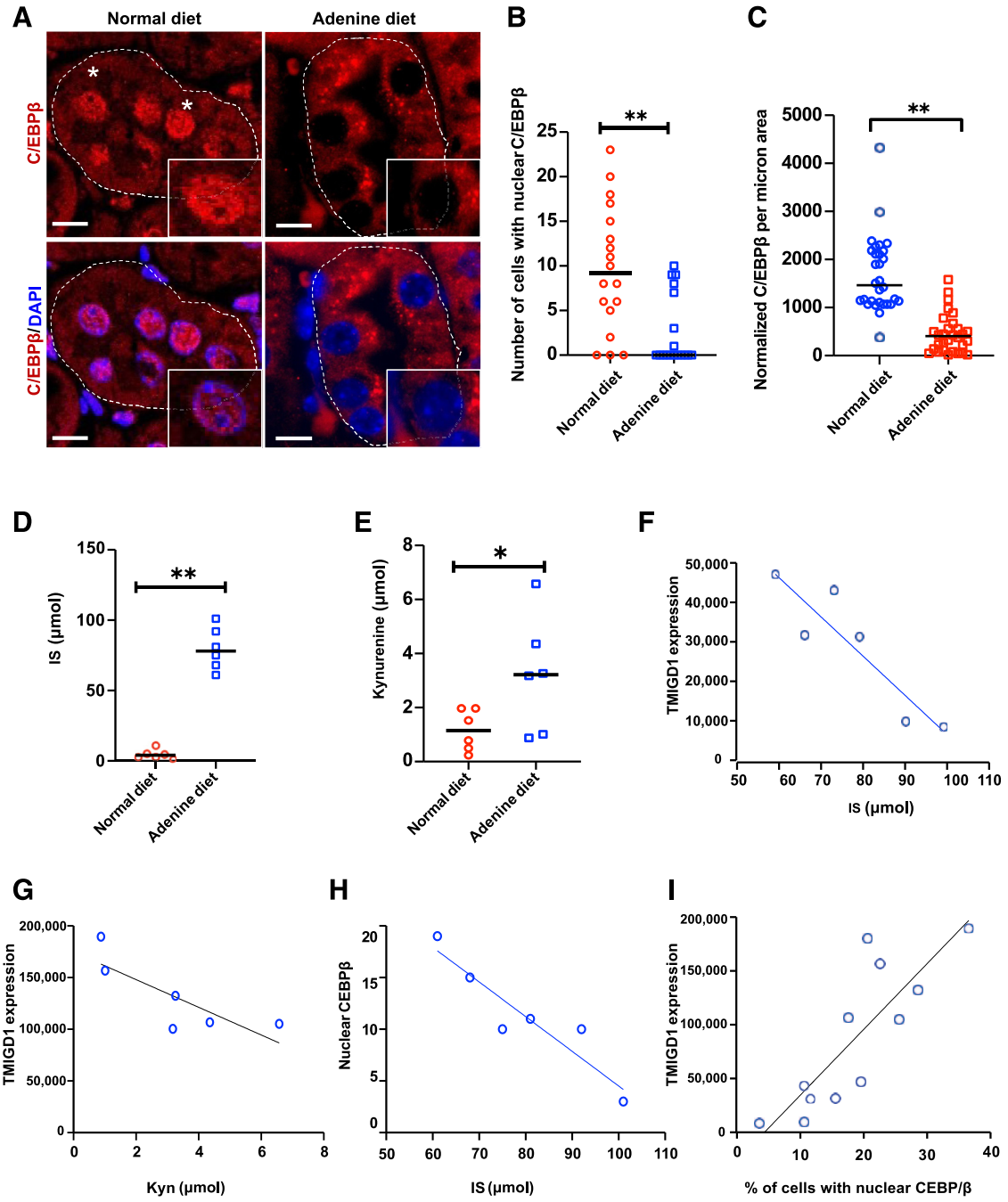

Figure 3 Down-regulation of CCAAT enhancer-binding protein β (C/EBPβ) in mice with adenine-induced chronic kidney disease, which correlates with the levels of indoxyl sulfate (IS) and kynurenine (Kyn). **A:** Kidneys harvested from the indicated groups of mice were stained with C/EBPβ antibody, followed by Alexa Fluor secondary antibody. DAPI stained nuclei. Representative images from kidneys from six mice per group are shown. The **white asterisks** are on tubular cells with nuclear C/EBPβ. **Insets:** C/EBPβ localization in a renal tubular cell. **White dotted lines** are the border of a tubule. **B:** The number of tubular cells with nuclear C/EBPβ staining was counted in five high-power fields in each mouse per group in controls and mice exposed to 0.2% adenine diet for the indicated period. The number of cells with the nuclear or cytosol C/EBPβ staining was counted in a manner blind to the sample. The *t*-test was used. The *P* value is given compared with the number of tubular cells with the nuclear C/EBPβ in the normal diet group. **C:** Normalized integrated density of C/EBPβ of kidney obtained from both the groups of mice. For each mouse, five high-power fields in each mouse per group in controls and mice exposed to a 0.2% adenine diet were analyzed. **D:** Serum IS levels in mice at the end of the experiment are shown. Groups were compared using the *t*-test. **E:** Serum Kyn levels in mice are shown. Groups were compared using the *t*-test. **F:** Ten randomly selected high-power fields of kidney tissues per mouse on an adenine diet and normal diet were used to estimate TMIGD1 expression as integrated density normalized to the surface area. The integrated density readings were averaged per mouse and correlated with the IS levels. $R^2 = 0.827$; $P = 0.0119$. **G:** The integrated density readings of TMIGD1 were correlated with the Kyn levels. $R^2 = 0.653$; $P = 0.051$. **H:** Average numbers of tubular cells with nuclear C/EBPβ per 10 images per mouse were used for this analysis. A linear regression was performed. $R^2 = 0.78$; $P = 0.0001$. **I:** A linear correlation analysis was performed between IS levels and TMIGD1 expression, as estimated by the intensity density normalized to the area from mice on an adenine diet. $R^2 = 0.55$; $P = 0.0511$. $N = 6$ per group (**B**, **C**, and **F**). $^*P < 0.05$, $^{**}P < 0.01$. Scale bar = 100 μm (**A**). Original magnification, ×100 (**A**).

Given the structural similarities of IS and other tryptophan metabolites, the authors hypothesized that tryptophan metabolites might similarly down-regulate TMIGD1 transcription. To this effect, HEK293T cells expressing TMIGD1 luciferase construct were exposed to physiologically relevant concentrations of Kyn, kynurenic acid, quinolinic acid, xanthurenic acid, anthranilic acid, and IA, and the luciferase signal was measured. The results showed that Kyn, kynurenic acid, and quinolinic acid had a dose-dependent down-regulation of TMIGD1 transcription (Supplemental Figure S3, A–C). However, the results did not show a dose-dependent down-regulation with anthranilic acid, xanthurenic acid, and IA treatments (Supplemental Figure S3, D–F). These findings were further validated in Kyn-treated cells using real-time RT-PCR. The results demonstrated a dose-dependent suppression of TMIGD1 mRNA in cells treated with Kyn at levels corresponding to patients with CKD (Supplemental Figure S3G). These results suggest that the suppressive effect on TMIGD1 transcription is not limited to IS but is also shared by some tryptophan metabolites.

These tryptophan-based uremic solutes are known to accumulate during CKD. Therefore, the authors posited that TMIGD1 expression would be suppressed in the renal tubules and that it would correlate with the levels of these uremic solutes. To explore this hypothesis, TMIGD1 expression was examined in different models of CKD. The adenine-induced CKD model is characterized by profound tubulointerstitial fibrosis inflicted by the deposition of 2,8-dihydroxy-adenine. This model is characterized by the retention of uremic toxins and recapitulates several manifestations of uremia, including osteodystrophy, uremic cachexia, and a hyper-thrombotic milieu.[11,17,18] A group of 8- to 12-week–old male and female C57BL/6 mice were exposed to a 0.2% adenine diet for 4 weeks. Hematoxylin and eosin–stained renal tissue showed prominent tubular dilatation, loss of tubular epithelial cells and brush border of proximal tubular epithelial cells, tubular cell atrophy, dilatation of tubules, and intraluminal casts, along with interstitial inflammation mice with adenine diet on hematoxylin and eosin staining (Figure 2A). Masson trichrome staining showed tubulointerstitial fibrosis in the adenine-exposed mice compared with controls (Figure 2B). IFTA is considered the universal pathologic characteristic implicated in the progression of CKD, irrespective of underlying causes.[19] The IFTA grading showed a fourfold increase in the IFTA scores in the adenine-exposed mice compared with controls (Figure 2C). BUN doubled in mice on an adenine diet compared with those on a normal diet (Figure 2D).

TMIGD1 was expressed in the cytosol and membrane of tubular cells in both the proximal and distal renal tubular epithelial cells (Supplemental Figure S4A), as indicated by immunofluorescence staining. Initial analysis suggested suppression of TMIGD1 in the intact tubules of mice with an adenine diet compared with that in controls (Figure 2E). Therefore, its expression in normally appearing tubules was quantified and presented as integrated density using ImageJ software. Integrated density represents a combination of intensity and number of pixels for a prespecified region of interest and normalizes to the surface area (in micrometers)[16,20] (Figure 2F). Because a decrease in the number of intact tubules with CKD can also result in a reduced expression of tubular proteins, the levels of TMIGD1 were normalized to intact tubules. As a result, compared with controls, a 3.6-fold reduction in normalized TMIGD1 expression was noted in the kidneys of mice exposed to an adenine diet. This finding was further confirmed in the renal lysates of mice in both groups (Figure 2, G and H), which showed a 2.5-fold suppression in TMIGD1 levels in mice on an adenine diet compared with those on a normal diet. Kidney whole cell lysates for Ksp-cadherin and N-cadherin were examined. A 40% to 60% down-regulation of both Ksp-cadherin and N-cadherin was observed in the kidneys of mice exposed to adenine diet compared with those exposed to normal diet (Supplemental Figure S4, B–E). Mice with adenine-induced CKD have IS levels of 75 to 100 μmol/L,[21] which was corroborated by the results in BUMPT cells (Supplemental Figure S1). N-cadherin was strikingly down-regulated in the adenine diet model. These data may suggest that N-cadherin in renal tubule is regulated by mechanisms or metabolites independent of IS.

The levels of C/EBPβ in the kidneys of control and adenine-exposed mice were congruent with that of TMIGD1. C/EBPβ was predominantly located in the nuclei of RTECs in the mice on a normal diet. Its expression was reduced and was observed in the cytosol in mice on an adenine diet (Figure 3A). This observation was further quantitated by counting the number of tubular cells positive for nuclear C/EBPβ. Five randomly obtained high-power field images from each mouse kidney were analyzed, and a few cells with nuclear C/EBPβ were counted in a blinded manner. In mice on a normal diet, 9.4 + 5.9 cells/high-power field had nuclear C/EBPβ, compared with 0 to 2 cells/high-power field in renal tubules of mice on an adenine diet (Figure 3B). The integrated density of C/EBPβ normalized to intact renal tubules showed threefold reduction of kidneys of mice on adenine diet compared with those on a normal diet (Figure 3C).

Metabolomics analysis showed a significant increase of IS and Kyn levels in mice on an adenine diet (Figure 3, D and E). Correlation analysis showed that blood levels of IS and Kyn negatively correlated with TMIGD1 expression [$R^2 = 0.827$ ($P = 0.0119$) and $R^2 = 0.653$ ($P = 0.051$), respectively] (Figure 3, F and G). IS levels negatively correlated with nuclear C/EBPβ (linear correlation coefficient $R^2 = 0.78$; $P = 0.0001$) (Figure 3H). Finally, TMIGD1 expression correlated positively with nuclear C/EBPβ (linear correlation coefficient $R^2 = 0.55$; $P = 0.0511$) (Figure 3I). Collectively, these results suggest that TMIGD1 expression correlates with C/EBPβ in the renal tubules and that IS and Kyn levels negatively correlate with the expressions of C/EBPβ and TMIGD1 in RTECs.

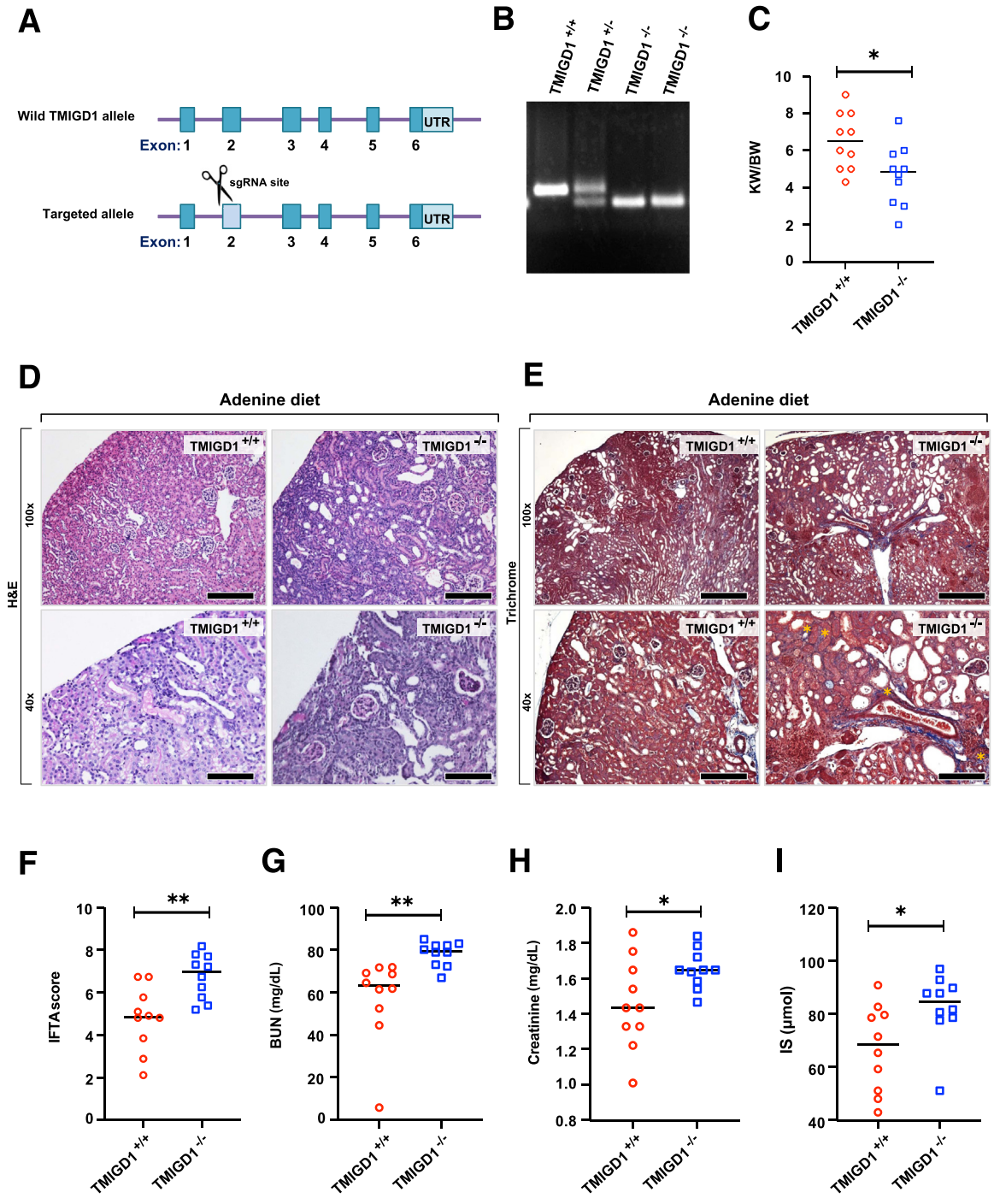

Figure 4 Global TMIGD1 knockout (KO) mice demonstrate more kidney injury in the adenine-induced chronic kidney disease model. **A:** A schema to generate TMIGD1 KO mice. **B:** Genotyping of TMIGD1 wild-type, heterozygous (+/−), and homozygous KO mice (−/−) is shown. **C:** A group of female TMIGD1 KO mice and littermate wild-type mice (controls) was subjected to a 0.2% adenine diet for 4 weeks. Kidneys harvested at the end of the experiment were weighed and presented as the ratio of kidney weight (KW)/total body weight (BW). The *t*-test was performed. **D:** Representative images of hematoxylin and eosin (H&E)—stained paraffin-embedded kidney sections from each mouse at two magnifications are shown. **E:** Representative images of modified Masson trichrome-stained paraffin-embedded kidney sections from each mouse at two magnifications are shown. **Yellow asterisks** depict the fibrotic area stained blue. **F:** Interstitial fibrosis and tubular atrophy (IFTA) score was measured for kidneys from each mouse per group in a manner blinded to the group. The *t*-test was performed. **G:** Serum blood urea nitrogen (BUN) values from each group exposed to an adenine diet for 3 weeks are shown. The *t*-test was performed. **H:** Serum creatinine values from each group exposed to an adenine diet for 3 weeks are shown. The *t*-test was performed. **I:** Serum indoxyl sulfate (IS) values from each group exposed to an adenine diet for 3 weeks are shown. The *t*-test was performed. $N = 10$ mice per group (**C**—**E**). $^{*}P < 0.05$, $^{**}P < 0.01$. Scale bars: 100 μm (**D** and **E**, **top panels**); 25 μm (**D** and **E**, **bottom panels**). Original magnifications: ×100 (**D** and **E**, **top panels**); ×40 (**D** and **E**, **bottom panels**). UTR, untranslated region.

Next, the relationships in the above paragraph were confirmed in other CKD models. Unilateral ureteral obstruction (UUO) is a well-established model of obstructive nephropathy.[19] From a group of 24 female C57Bl6 mice, six mice were harvested per week for 3 weeks, and six more mice were reserved as sham-operated controls. The numbers of cells with nuclear C/EBPβ and C/EBPβ levels were quantified in the kidneys of mice using IF (Supplemental Figure S5A). A strong negative correlation was noted between weeks of UUO and the number of renal tubular cells with nuclear C/EBPβ ($R^2 = 0.48$; $P = 0.007$) (Supplemental Figure S5B) and TMIGD1 levels in the intact tubular cells ($R^2 = 0.41$; $P = 0.01$) (Supplemental Figure S5C). Similar findings were noted in the DOCA-salt nephrectomy model, an established model of hypertensive nephropathy. Ten female C57Bl6 mice underwent unilateral nephrectomy and DOCA-salt implantation, whereas five sham-operated mice served as controls. The number of renal tubular cells with nuclear C/EBPβ and TMIGD1 expression was significantly reduced in DOCA-salt nephrectomy mice compared with controls (Supplemental Figure S5, D–F).

All of the models in the previous paragraph indicate a reduction in TMIGD1 expression in the renal tubules of mice with CKD and its strong inverse correlation with IS and Kyn. These results suggest an association between TMIGD1 and renal tubular damage. To establish causality, a global TMIGD1 KO mouse line was generated and these mice were subjected to CKD, hypothesizing that TMIGD1 loss would exacerbate renal tubular damage and worsen renal function.

The homozygous global TMIGD1$^{-/-}$ mice were generated via clustered regularly interspaced short palindromic repeats (CRISPR)-Cas 9 system (Figure 4A). CRISPR-Cas 9–mediated loss of TMIGD1 was confirmed by real-time quantitative PCR (Figure 4B). TMIGD1 KO mice on a C57BL6 background are viable and fertile, and pups display no abnormality at the baseline. Kidney sections of TMIGD1$^{-/-}$ mice showed no evidence of change compared with wild-type littermates. A group of TMIGD1$^{-/-}$ mice was subjected to a 0.2% adenine-induced CKD model for 4 weeks. Cohoused wild-type littermates served as controls. TMIGD1$^{-/-}$ mice had lower kidney weight compared with TMIGD1$^{+/+}$ mice, as represented by a ratio between the kidney and total body weight, suggestive of a loss of functional kidney mass (Figure 4C). The kidney sections from these mice showed higher tubular atrophy, dilated tubules, and glomerulosclerosis compared with the wild-type controls (Figure 4D). Masson trichrome stain showed fibrosis in the perivascular and medullary regions in TMIGD1$^{-/-}$ mice (Figure 4E). A 1.5-fold increase in the IFTA score was noted in TMIGD1$^{-/-}$ kidneys compared with controls (Figure 4F). BUN and creatinine had increased by 40% to 50% in TMIGD1$^{-/-}$ mice. Average BUN was 60 mg/dL in the TMIGD1$^{+/+}$ mice versus 78 mg/dL in the TMIGD1$^{-/-}$ mice (Figure 4G). Average creatinine levels in the TMIGD1$^{+/+}$ mice were 1.4 mg/dL, which increased to 1.6 mg/dL in the TMIGD1$^{-/-}$ mice (Figure 4H). Furthermore, the average level of IS increased to 82 μmol/L compared with 65 μmol/L in the TMIGD1$^{+/+}$ mice (Figure 4I). On adenine diet, TMIGD1$^{+/-}$ mice showed greater tubular atrophy and fibrosis compared with wild-type littermates on adenine diet (Supplemental Figure S6).

TMIGD1$^{-/-}$ mice subjected to two different animal models recapitulated similar findings as the adenine-induced CKD model. A group of 8- to 12-week–old female C57Bl6 TMIGD1$^{+/+}$ and TMIGD1$^{-/-}$ mice was subjected to the UUO model. Five mice were harvested at baseline and weekly to the third week after UUO. Both TMIGD1$^{+/+}$ and TMIGD1$^{-/-}$ mice showed increased fibrosis in the remaining kidney with the UUO model, which was apparent in the second week (Figure 5A). TMIGD1$^{-/-}$ kidney showed an atrophied cortex by the third week. The IFTA score increased in the second and third weeks in TMIGD1$^{-/-}$ mice compared with TMIGD1$^{+/+}$ mice (Figure 5B). Similarly, BUN increased by 32% to 40% in TMIGD1$^{-/-}$ mice in the second and third weeks (Figure 5C). The DOCA-salt unilateral nephrectomy model is a well-established model of hypertensive renal disease with loss of functional nephron mass.[19] In the DOCA-salt unilateral nephrectomy model, TMIGD1$^{-/-}$ mice kidneys showed greater tubular atrophy and interstitial fibrosis (Figure 5D). The IFTA score increased in the control kidneys from 2.5 to 3.8 in the TMIGD1$^{-/-}$ mice with the DOCA-salt nephrectomy model (Figure 5E). BUN showed a similar trend and increased from 27 to 40 mg/dL (Figure 5F). Collectively, this set of data shows that TMIGD1$^{-/-}$ mice have greater tubular damage and worse renal function than TMIGD1$^{+/+}$ mice.

Potential mechanism of TMIGD1 regulating tubular survival was examined further. Previous work has shown that TMIGD1 regulates acetylation of tubulin,[22] which is necessary for spindle formation during mitosis of cellular proliferation.[8,23] The authors hypothesized that loss of TMIGD1 will reduce acetylated tubulin levels and tubular cell proliferation. To investigate this hypothesis, TMIGD1$^{-/-}$ and TMIGD1$^{+/-}$ mice were subjected to a 0.2% adenine diet for 2 weeks to induce renal tubular damage and proliferation of cells. TMIGD1$^{+/+}$ mice on an adenine diet and mice on normal diet served as controls (Figure 6A). In the normal diet group, no change in acetylated tubulin expression was noted between three groups (Supplemental Figure S7). On an adenine diet, TMIGD1$^{+/+}$ mice had prominently acetylated tubulin in proximal tubular cells. Compared with this control, TMIGD1$^{-/-}$ and TMIGD1$^{+/-}$ mice had lower expression of acetylated tubulin levels in proximal tubular cells. Integrated density analysis revealed that, compared with TMIGD1$^{+/+}$ mice, TMIGD1$^{+/-}$ and TMIGD1$^{-/-}$ mice showed 22% and 90% reduction in the expression of acetylated tubulin, respectively (Figure 6B).

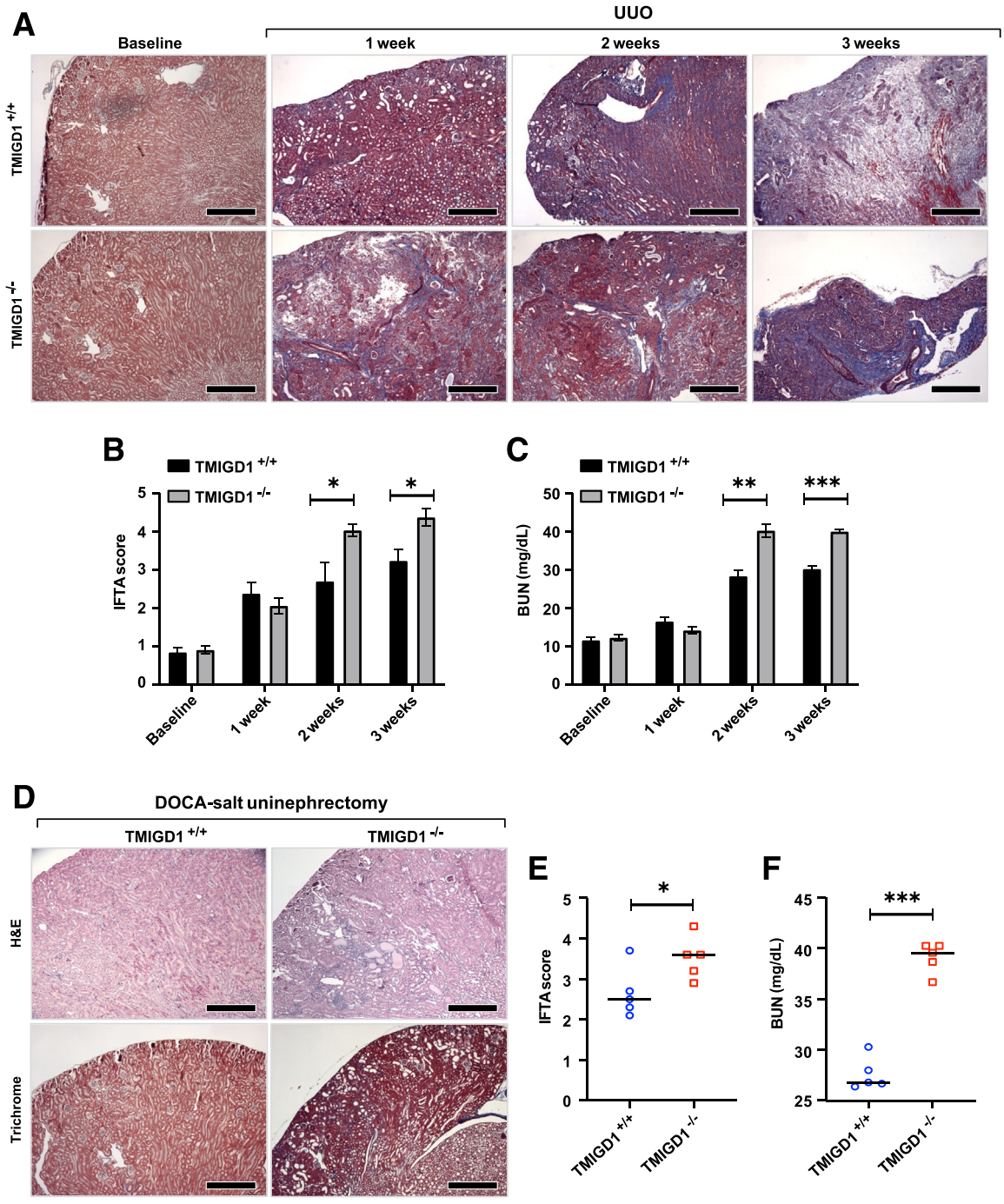

Figure 5 TMIGD1 knockout mice demonstrate greater tubular injury in unilateral ureteral obstruction (UUO) and deoxycorticosterone acetate (DOCA) nephrectomy chronic kidney disease models. **A:** A group of 15 C57BL/6 TMIGD1$^{-/-}$ mice and 15 TMIGD$^{+/+}$ littermates were subjected to the UUO model, of which five mice were harvested every week. Sham-operated mice served as controls. Kidneys stained with modified Masson trichrome stain are shown. **B:** Interstitial fibrosis and tubular atrophy (IFTA) score was measured for kidneys from each mouse per group in a manner blinded to the group. Analysis of variance (ANOVA) was performed to compare all the groups ($P = 0.001$). Groups were compared using an independent *t*-test. *P* values are shown after 2 and 3 weeks. **C:** Serum blood urea nitrogen (BUN) values from each group are shown. ANOVA was performed to compare all the groups ($P = 0.006$). Groups were compared using an independent *t*-test. *P* values are shown after 2 and 3 weeks. **D:** A group of five C57BL/6 TMIGD1$^{-/-}$ mice and 15 TMIGD$^{+/+}$ littermates were subjected to unilateral nephrectomy and DOCA-salt table implantation model. Representative images of kidneys stained with hematoxylin and eosin (H&E) and modified Masson trichrome stain from each group are shown. **E:** IFTA score was measured for kidneys from each mouse per group in a manner blinded to the group. Groups were compared using the *t*-test. **F:** Serum BUN values from each group are shown. Groups were compared using the *t*-test. $N = 5$ per group (**A**, sham-operated mice). $^{*}P < 0.05$, $^{**}P < 0.01$, and $^{***}P < 0.001$. Scale bars = 25 μm (**A** and **D**). Original magnification, ×40 (**A** and **D**).

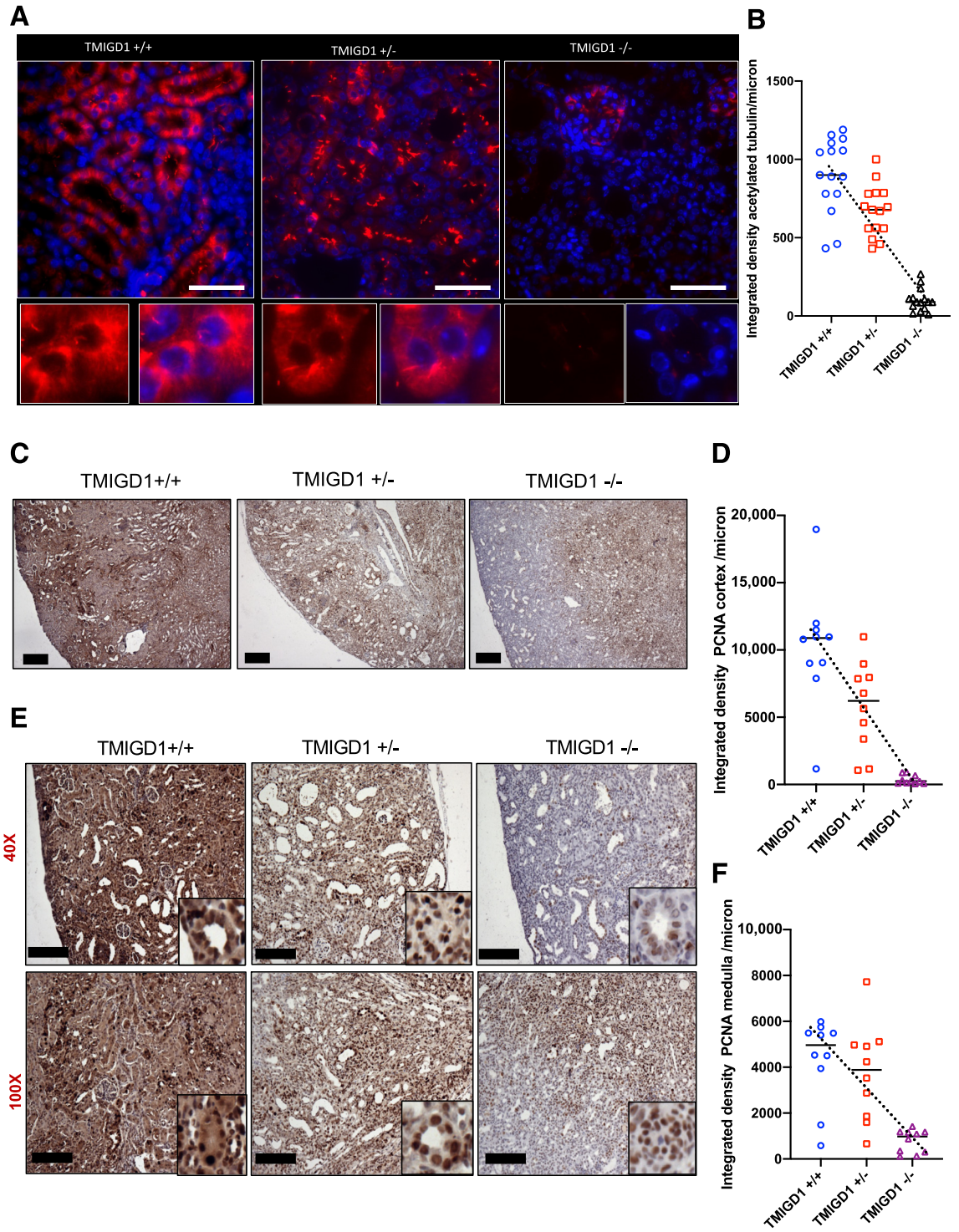

Figure 6 TMIGD1 knockout reduces acetylated tubulin and cell proliferation. **A:** Kidneys harvested from the indicated groups of mice on a 0.2% adenine diet for 2 weeks were stained with acetylated tubulin antibody. DAPI stained nuclei. Representative images from kidneys from five mice per group are shown. **Bottom:** Tubular cells with acetylated tubulin. **B:** Normalized integrated density of acetylated tubulin obtained from three groups of mice. Three high-power fields in each mouse per group were analyzed. A linear regression was performed. $R^2 = 0.71$; and $P = 0.004$. **C:** Kidneys harvested from the indicated groups of mice on a 0.2% adenine diet for 2 weeks were stained with proliferating cell nuclear antigen (PCNA). DAPI stained nuclei. Representative images from kidneys from five mice per group are shown. **D:** Normalized integrated density of PCNA obtained from three groups of mice. Two random fields in each mouse per group were analyzed. A linear regression was performed. $R^2 = 0.83$; $P < 0.001$. **E:** Kidneys harvested from the indicated mice in the adenine group were stained with PCNA. DAPI stained nuclei. Images of medulla are shown. Representative images from kidneys from five mice per group are shown. **Insets:** PCNA-positive tubular cells. **F:** Normalized integrated density of PCNA obtained from three groups of mice. Two random fields in each mouse per group were analyzed. A linear regression was performed. $R^2 = 0.68$; and $P = 0.010$. $N = 5$ mice per group (**B**, **D**, and **F**). Scale bars: 100 μm (**A** and **E**, **bottom panels**); 50 μm (**C** and **E**, **top panels**). Original magnifications: ×100 (**A** and **E**, **bottom panels**); ×40 (**C**, cortex, and **E**, **top panels**).

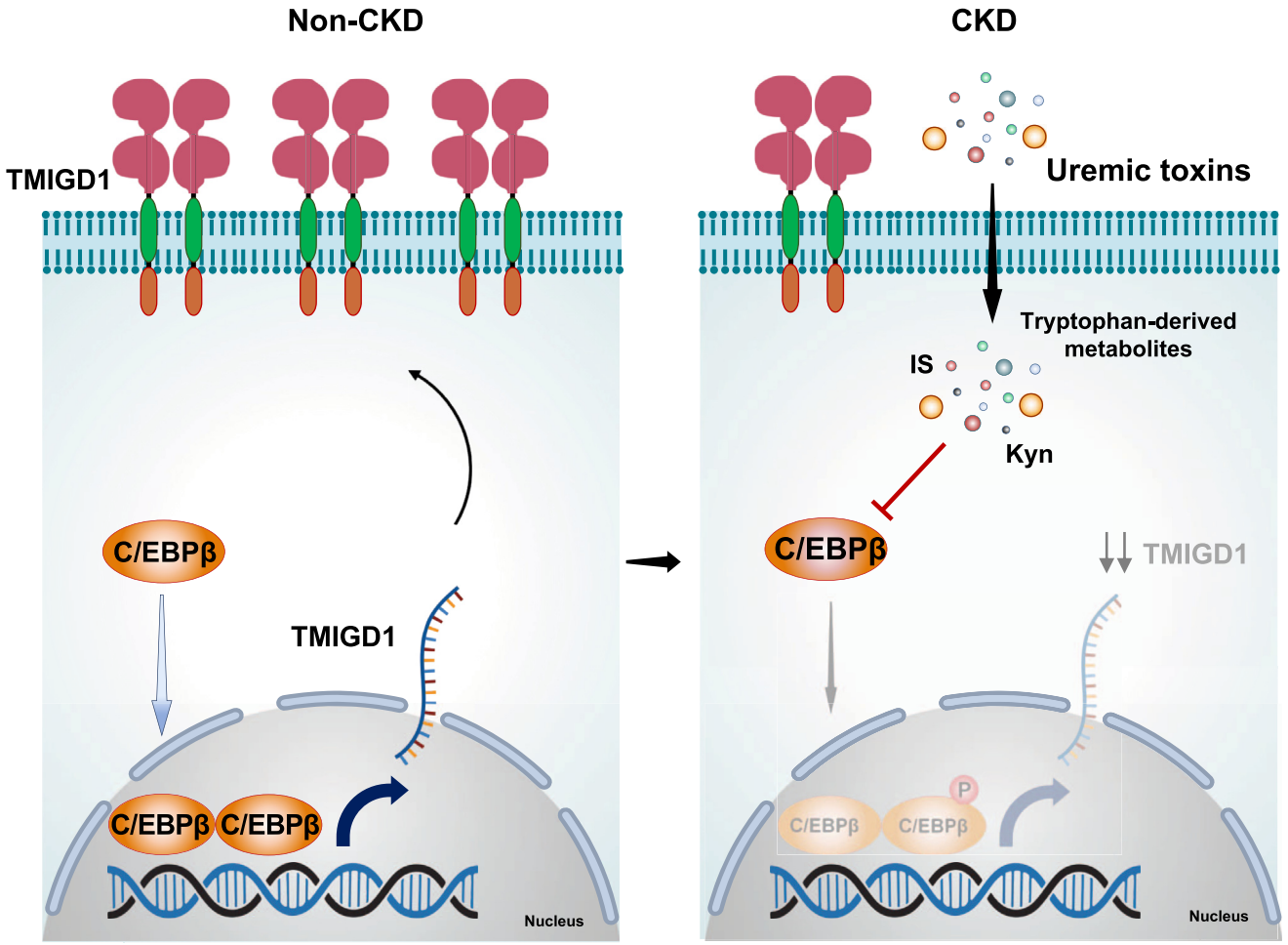

Figure 7 Proposed model of uremic solutes—CCAAT enhancer-binding protein β (C/EBPβ)—TMIGD1 axis for renal tubular cell protection. In normal renal function, C/EBPβ increases the transcription of TMIGD1 in the renal tubular cells. With tubular damage, accumulation of a set of tryptophan metabolites reduces the expression of C/EBPβ, which, in turn, suppresses TMIGD1 levels in tubules. Along with our previous work, these data suggest that down-regulation of TMIGD1 in the uremic milieu further compromises tubular cell survival. CKD, chronic kidney disease; IS, indoxyl sulfate; Kyn, kynurenine.

PCNA and Ki-67, well-established cell proliferation markers, were examined further in both the cortex and medulla. These regions were examined separately as differences were noted in cell proliferation markers in between the cortex and medulla. In the adenine diet group, TMIGD1$^{-/-}$ and TMIGD1$^{+/-}$ mice showed lower PCNA in the cortex compared with TMIGD1$^{+/+}$ mice (Figure 6, C and D). The tubular cell proliferation in the medulla was lower than in the cortex. A similar reduction in PCNA expression was noted in the medulla of TMIGD1$^{-/-}$ and TMIGD1$^{+/-}$ mice compared with the controls, with TMIGD1$^{-/-}$ mice showing minimal PCNA expression (Figure 6, D–F). Ki-67 expression pattern was like that of PCNA in TMIGD1$^{+/+}$, TMIGD1$^{-/-}$, and TMIGD1$^{+/-}$ mice on adenine diet (Supplemental Figure S8). These results suggest that loss of TMIGD1 reduces acetylated tubules and compromises tubular cell proliferation.

Discussion

This work demonstrates the down-regulation of TMIGD1 expression in different CKD models. This effect is, in part, driven by the accumulated tryptophan-derived uremic toxins, such as IS and Kyn. This event suppresses C/EBPβ-mediated TMIGD1 transcription in the renal tubular epithelial cells. The study demonstrated that the *in vivo* significance of TMIGD1. TMIGD1 KO mice show greater renal tubular damage and worse renal function in different CKD models. Loss of TMIGD1 decreased acetylated tubulin expression and tubular cell proliferation. Combined with previous work,[8] the data support an IS-CCAAT/EBPβ-TMIGD1 axis in renal tubules and a model of IS- and Kyn-induced tubulotoxicity (Figure 7). These data suggest that CKD (from an inciting cause) results in the accumulation of uremic toxins, such as IS and Kyn. Higher levels of IS and Kyn suppress the C/EBPβ-TMIGD1 axis, compromising renal tubular cell

survival and perpetuating the decline of renal function. These results also suggest that the down-regulation of TMIGD1 expression in the renal tubules in CKD model is not due to reduction in renal tubular mass but rather that TMIGD1 down-regulation contributes to renal tubular loss.

The normal kidney contains post-mitotic quiescent renal tubular cells in the G_0 phase with a low turnover.[24] The proliferation of renal tubular cells is essential for the regeneration of renal tubules after an insult. Renal tubular cells undergo several processes to regenerate tubules, including dedifferentiation, proliferation, and redifferentiation, to acquire the tubular cell phenotype.[24] Mitotic spindle assembly is critical for cell division.[25] Previous work has shown that TMIGD1 binds to the ezrin, radixin, and moesin family proteins in renal tubular epithelial cells (namely, moesin and ezrin).[22] Moesin primarily interacts with TMIGD1 via its N-terminal domain. Loss of moesin impairs the TMIGD1-mediated acetylation of α-tubulin and F-actin and mitotic spindle organization. Loss of TMIGD1 regulation of lysine 40 acetylation (K40) of microtubules, mitotic spindle formation, and cell proliferation is likely to be one of the mechanisms driving renal tubular damage in CKD models.

A dichotomy in the function of TMIGD1 exists. In von Hippel–Lindau null renal proximal tubular epithelial cells, TMIGD1 stimulates phosphorylation of p38 mitogen-activated protein kinases (MAPK) and induces the expression of p21 cyclin-dependent kinase inhibitor 1 and p27 cyclin-dependent kinase inhibitor 1B.[9] These events attribute to the tumor suppressor function of TMIGD1, suggesting that TMIGD1 may have different roles in normal versus transformed renal tubular epithelial cells with the loss of tumor suppressor.

TMIGD1 has been shown to protect renal tubules against oxidative stress and nutrient deprivation.[8] Several studies have demonstrated that the uremic milieu is highly oxidative,[26] and IS induces oxidative stress in different cells.[27–29] Therefore, it stands to reason that pro-oxidative uremic solutes target TIMGD1 and suppress its expression. Indoxyl sulfate is a decomposition product of tryptophan by intestinal bacteria and liver metabolism. IS is associated with different pathologic processes in renal tubules, such as oxidative stress, inflammation, epithelial-to-mesenchymal transition, and apoptosis of renal tubular cells.[30–35] However, the mediators of these effects remain incompletely understood. This work supports the notion that down-regulation of TMIGD1 is one of the mediators of IS-induced tubulotoxicity (Figure 7). Moreover, this work expands TMIGD1 transcriptional regulation by other tryptophan metabolites, such as IA, Kyn, and kynurenic acid, possibly due to shared structural elements with IS, such as indole and cyclopentane rings. This work proposes a potential role of other tryptophan metabolites in tubular toxicity.

The C/EBP proteins, a family of transcription factors, bind to nonsymmetric DNA sequences in the promoter/enhancer regions to regulate various functions, such as cell cycle, inflammation, metabolism, and host immune responses. C/EBP members are linked to renal diseases. Xie et al[36] described that fibrosis in the UUO model is characterized by the down-regulation of tubulointerstitial nephritis antigen in the obstructed kidney. C/EBPβ binds to the tubulointerstitial nephritis antigen promoter to regulate its expression. Duitman et al[37] demonstrated that C/EBPδ deficiency increased renal fibrotic response, enhanced tubular injury, increased collagen deposition in the interstitial area, and produced a higher expression of transforming growth factor-β in the UUO model. The current work adds to these previous reports and links TMIGD1 and uremic solutes to C/EBP biology.

This work has limitations. Cell division may be oriented longitudinal (apical-basal) or perpendicular to it in tubules.[25] Further work is needed to examine the TMIGD1 regulation of mitotic spindles in renal tubules after injury and the mechanism of down-regulation of C/EBPβ by uremic toxins. This study focused on CKD models in female mice. The current models do not investigate the role of TMIGD1 in the transition from acute kidney injury to CKD in both sexes.

In conclusion, the current work demonstrated the renoprotective role of TMIGD1 in various CKD models and uncovered a mechanism of tubulotoxicity by tryptophan-derived uremic toxins. This work supports further exploration of TMIGD1 as a potential therapeutic target to protect renal tubules in CKD.

Acknowledgments

We thank Dr. Michael Kirber (Boston University Medical Center Imaging Core facility) for assistance with confocal microscopy; Manisha Cole (Boston University School of Medicine) for technical assistance; and the Boston University Chemistry Instrumentation Core for the metabolomics analysis of the samples.

Author Contributions

V.C.C. and N.R. conceived the study; V.C.C., N.R., M.B., and W.Y. designed the research; M.B., W.Y., X.Y., and S.L. generated the mouse models; N.R. generated human recombinant FC-TMIGD1 protein; R.D.M. generated promoter-receptor construct; W.Y., M.A.N., I.E.S., E.M., S.L., and M.B. performed cell-based and animal experiments; V.C.C., W.Y., M.A.N., I.E.S., and M.B. performed immunofluorescence studies; A.V. generated data; S.A.W. and N.L. performed metabolomics analysis; X.Y., A.Z., and A.J. provided scientific input; V.C.C., I.E.S., M.B., and W.Y. prepared the manuscript; and the remaining authors including A.J. and A.Z. provided comments on the manuscript.

Supplemental Data

Supplemental material for this article can be found at *http://doi.org/10.1016/j.ajpath.2023.06.018*.

References

1. Centers for Disease Control and Prevention: Chronic Kidney Disease in the United States, 2019. Atlanta, GA, US Department of Health and Human Services, Centers for Disease Control and Prevention, 2019
2. Hill NR, Fatoba ST, Oke JL, Hirst JA, O'Callaghan CA, Lasserson DS, Hobbs FDR: Global prevalence of chronic kidney disease - a systematic review and meta-analysis. PLoS One 2016, 11: e0158765
3. Vanholder R: Introduction to the toxins special issue on "novel issues in uremic toxicity.". Toxins (Basel) 2018, 10:388
4. Goek ON, Doring A, Gieger C, Heier M, Koenig W, Prehn C, Romisch-Margl W, Wang-Sattler R, Illig T, Suhre K, Sekula P, Zhai G, Adamski J, Kottgen A, Meisinger C: Serum metabolite concentrations and decreased GFR in the general population. Am J Kidney Dis 2012, 60:197−206
5. Rhee EP, Clish CB, Ghorbani A, Larson MG, Elmariah S, McCabe E, Yang Q, Cheng S, Pierce K, Deik A, Souza AL, Farrell L, Domos C, Yeh RW, Palacios I, Rosenfield K, Vasan RS, Florez JC, Wang TJ, Fox CS, Gerszten RE: A combined epidemiologic and metabolomic approach improves CKD prediction. J Am Soc Nephrol 2013, 24: 1330−1338
6. Wu IW, Hsu KH, Lee CC, Sun CY, Hsu HJ, Tsai CJ, Tzen CY, Wang YC, Lin CY, Wu MS: p-Cresyl sulphate and indoxyl sulphate predict progression of chronic kidney disease. Nephrol Dial Transplant 2011, 26:938−947
7. Ravid JD, Kamel MH, Chitalia VC: Uraemic solutes as therapeutic targets in CKD-associated cardiovascular disease. Nat Rev Nephrol 2021, 17:197−206
8. Arafa E, Bondzie PA, Rezazadeh K, Meyer RD, Hartsough E, Henderson JM, Schwartz JH, Chitalia V, Rahimi N: TMIGD1 is a novel adhesion molecule that protects epithelial cells from oxidative cell injury. Am J Pathol 2015, 185:2757−2767
9. Meyer RD, Zou X, Ali M, Ersoy E, Bondzie PA, Lavaei M, Alexandrov I, Henderson J, Rahimi N: TMIGD1 acts as a tumor suppressor through regulation of p21Cip1/p27Kip1 in renal cancer. Oncotarget 2018, 9:9672−9684
10. Woolf N, Meyer RD, Bondzie PA, Xu HH, Rahimi N: Cell adhesion molecule TMIGD1 is downregulated in advanced colorectal adenocarcinoma. Modern Pathol 2017, 30:207a
11. Shashar M, Belghasem ME, Matsuura S, Walker J, Richards S, Alousi F, Rijal K, Kolachalama VB, Balcells M, Odagi M, Nagasawa K, Henderson JM, Gautam A, Rushmore R, Francis J, Kirchhofer D, Kolandaivelu K, Sherr DH, Edelman ER, Ravid K, Chitalia VC: Targeting STUB1-tissue factor axis normalizes hyperthrombotic uremic phenotype without increasing bleeding risk. Sci Transl Med 2017, 9:1−11
12. Patel VA, Lee DJ, Feng L, Antoni A, Lieberthal W, Schwartz JH, Rauch J, Ucker DS, Levine JS: Recognition of apoptotic cells by epithelial cells: conserved versus tissue-specific signaling responses. J Biol Chem 2010, 285:1829−1840
13. Kim JY, Silvaroli JA, Martinez GV, Bisunke B, Luna Ramirez AV, Jayne LA, Feng M, Girotra B, Acosta Martinez SM, Vermillion CR, Karel IZ, Ferrell N, Weisleder N, Chung S, Christman JW, Brooks CR, Madhavan SM, Hoyt KR, Cianciolo RE, Satoskar AA, Zepeda-Orozco D, Sullivan JC, Davidson AJ, Bajwa A, Pabla NS: Zinc finger protein 24-dependent transcription factor SOX9 upregulation protects tubular epithelial cells during acute kidney injury. Kidney Int 2023, 103:1093−1104
14. Yin L, Li H, Liu Z, Wu W, Cai J, Tang C, Dong Z: PARK7 protects against chronic kidney injury and renal fibrosis by inducing SOD2 to reduce oxidative stress. Front Immunol 2021, 12:690697
15. Chen HH, Lan YF, Li HF, Cheng CF, Lai PF, Li WH, Lin H: Urinary miR-16 transactivated by C/EBPbeta reduces kidney function after ischemia/reperfusion-induced injury. Sci Rep 2016, 6:27945
16. Arinze NV, Yin W, Lotfollahzadeh S, Napoleon MA, Richards S, Walker JA, Belghasem M, Ravid JD, Hassan Kamel M, Whelan SA, Lee N, Siracuse JJ, Anderson S, Farber A, Sherr D, Francis J, Hamburg NM, Rahimi N, Chitalia VC: Tryptophan metabolites suppress Wnt pathway and promote adverse limb events in CKD patients. J Clin Invest 2021, 132:e142260
17. Kolachalama VB, Shashar M, Alousi F, Shivanna S, Rijal K, Belghasem ME, Walker J, Matsuura S, Chang GH, Gibson CM, Dember LM, Francis JM, Ravid K, Chitalia VC: Uremic solute-aryl hydrocarbon receptor-tissue factor axis associates with thrombosis after vascular injury in humans. J Am Soc Nephrol 2018, 29: 1063−1072
18. Jia T, Olauson H, Lindberg K, Amin R, Edvardsson K, Lindholm B, Andersson G, Wernerson A, Sabbagh Y, Schiavi S, Larsson TE: A novel model of adenine-induced tubulointerstitial nephropathy in mice. BMC Nephrol 2013, 14:116
19. Yang HC, Zuo Y, Fogo AB: Models of chronic kidney disease. Drug Discov Today Dis Models 2010, 7:13−19
20. Belghasem M, Roth D, Richards S, Napolene MA, Walker J, Yin W, Arinze N, Lyle C, Spencer C, Francis JM, Thompson C, Andry C, Whelan SA, Lee N, Ravid K, Chitalia VC: Metabolites in a mouse cancer model enhance venous thrombogenicity through the aryl hydrocarbon receptor-tissue factor axis. Blood 2019, 134:2399−2413
21. Kim K, Anderson EM, Thome T, Lu G, Salyers ZR, Cort TA, O'Malley KA, Scali ST, Ryan TE: Skeletal myopathy in CKD: a comparison of adenine-induced nephropathy and 5/6 nephrectomy models in mice. Am J Physiol Renal Physiol 2021, 321: F106−F119
22. Rahimi N, Ho RXY, Chandler KB, De La Cena KOC, Amraei R, Mitchel AJ, Engblom N, Costello CE: The cell adhesion molecule TMIGD1 binds to moesin and regulates tubulin acetylation and cell migration. J Biomed Sci 2021, 28:61
23. Schatten G, Simerly C, Asai DJ, Szoke E, Cooke P, Schatten H: Acetylated alpha-tubulin in microtubules during mouse fertilization and early development. Dev Biol 1988, 130:74−86
24. Thomasova D, Anders HJ: Cell cycle control in the kidney. Nephrol Dial Transplant 2015, 30:1622−1630
25. Gao L, Yang Z, Hiremath C, Zimmerman SE, Long B, Brakeman PR, Mostov KE, Bryant DM, Luby-Phelps K, Marciano DK: Afadin orients cell division to position the tubule lumen in developing renal tubules. Development 2017, 144:3511−3520
26. Rysz J, Franczyk B, Lawinski J, Gluba-Brzozka A: Oxidative stress in ESRD patients on dialysis and the risk of cardiovascular diseases. Antioxidants (Basel) 2020, 9:1079
27. Muteliefu G, Enomoto A, Niwa T: Indoxyl sulfate promotes proliferation of human aortic smooth muscle cells by inducing oxidative stress. J Ren Nutr 2009, 19:29−32
28. Yang K, Xu X, Nie L, Xiao T, Guan X, He T, Yu Y, Liu L, Huang Y, Zhang J, Zhao J: Indoxyl sulfate induces oxidative stress and hypertrophy in cardiomyocytes by inhibiting the AMPK/UCP2 signaling pathway. Toxicol Lett 2015, 234:110−119
29. Tanaka H, Komaba H, Koizumi M, Kakuta T, Fukagawa M: Role of uremic toxins and oxidative stress in the development of chronic kidney disease-mineral and bone disorder. J Ren Nutr 2012, 22: 98−101
30. Ellis RJ, Small DM, Ng KL, Vesey DA, Vitetta L, Francis RS, Gobe GC, Morais C: Indoxyl sulfate induces apoptosis and hypertrophy in human kidney proximal tubular cells. Toxicol Pathol 2018, 46:449−459
31. Sun CY, Hsu HH, Wu MS: p-Cresol sulfate and indoxyl sulfate induce similar cellular inflammatory gene expressions in cultured proximal renal tubular cells. Nephrol Dial Transplant 2013, 28: 70−78
32. Shimizu H, Bolati D, Higashiyama Y, Nishijima F, Shimizu K, Niwa T: Indoxyl sulfate upregulates renal expression of MCP-1 via production of ROS and activation of NF-kappaB, p53, ERK, and JNK in proximal tubular cells. Life Sci 2012, 90:525−530

33. Bolati D, Shimizu H, Higashiyama Y, Nishijima F, Niwa T: Indoxyl sulfate induces epithelial-to-mesenchymal transition in rat kidneys and human proximal tubular cells. Am J Nephrol 2011, 34:318–323
34. Kawakami T, Inagi R, Wada T, Tanaka T, Fujita T, Nangaku M: Indoxyl sulfate inhibits proliferation of human proximal tubular cells via endoplasmic reticulum stress. Am J Physiol Renal Physiol 2010, 299:F568–F576
35. Taki K, Nakamura S, Miglinas M, Enomoto A, Niwa T: Accumulation of indoxyl sulfate in OAT1/3-positive tubular cells in kidneys of patients with chronic renal failure. J Ren Nutr 2006, 16: 199–203
36. Xie P, Sun L, Nayak B, Haruna Y, Liu FY, Kashihara N, Kanwar YS: C/EBP-beta modulates transcription of tubulointerstitial nephritis antigen in obstructive uropathy. J Am Soc Nephrol 2009, 20:807–819
37. Duitman J, Borensztajn KS, Pulskens WP, Leemans JC, Florquin S, Spek CA: CCAAT-enhancer binding protein delta (C/EBPdelta) attenuates tubular injury and tubulointerstitial fibrogenesis during chronic obstructive nephropathy. Lab Invest 2014, 94:89–97